ISIJ International, Vol. 60 (2020), No. 1, pp. 65–72

Thermal Decomposition Reaction Kinetics of Hematite Ore

Zhiyuan CHEN,[1)]* Christiaan ZEILSTRA,[2)] Jan VAN DER STEL,[2)] Jilt SIETSMA[1)] and Yongxiang YANG[1)]

1) Department of Materials Science and Engineering, Delft University of Technology, Mekelweg 2, 2628 CD Delft, The Netherlands.
2) Tata Steel Europe, PO Box 10000, 1970 CA IJmuiden, The Netherlands.

(*Received on March 1, 2019; accepted on July 16, 2019; J-STAGE Advance published date: September 19, 2019*)

In order to understand the thermal decomposition kinetics of hematite particles in inert atmosphere, thermogravimetriy was employed for isoconversional analysis. The kinetic triplet was estimated from the experimental data and the isothermal reaction kinetics was predicted. The results indicated that the thermal decomposition could be divided into two stages, of which the activation energies were 636 kJ/mol and 325 kJ/mol, respectively. The exponential form of pre-exponential factor, $\ln(A/s^{-1})$, for the two stages were estimated to be 42.9±6.6 and 14.1±3.08. At last, the kinetic mechanism of the first stage was suggested to match Sestak-Berggren model as $f(\alpha)=(1-\alpha)^{1.38}$. The relatively slow reaction rate of the second stage was due to the slag formation during the reaction.

KEY WORDS: isoconversional kinetics; iron oxide; hematite; thermal decomposition; HIsarna.

1. Introduction

Thermal decomposition of hematite requires relatively high temperature and can happen in non-reducing atmosphere, which is beyond most of the previous studies[1–5] of iron oxides reduction. The reduction kinetics of hematite in reducing gas is studied with the background of blast furnace process, chemical looping combustion and so on. Corresponding to the operation condition of these processes, the reaction temperature is usually controlled below 1 200°C in the previous studies. However, the development of the HIsarna process, a promising alternative ironmaking process,[6] requires the knowledge of reduction kinetics of hematite ore particles at the high temperatures. The HIsarna reactor contains two parts, the smelting reduction vessel (SRV) and the smelt cyclone. The reaction in SRV generates gas at around 1 400–1 450°C to the smelt cyclone,[7] where the hematite particles are heated up and pre-reduced as in suspension. Afterwards, the pre-reduced particles form slag, hit the wall of cyclone and flow down the wall to the SRV. At such high temperature, the pre-reduction of hematite is driven by chemical reduction by gas and thermal decomposition.

Most studies in this temperature range focused on the reduction of iron bearing slag,[8,9] magnetite[10,11] and wüstite[12,13] in reducing gas. Qu *et al.*[14–16] studied the reduction kinetics of hematite particles in reducing gas in detail, providing kinetic parameters and other relevant information. The kinetic details of thermal decomposition of hematite are still not clear although some key information has already been surveyed. Recently, Salmani *et al.*[17] studied the thermal decomposition kinetics of fine high-grade hematite powder at the high temperatures. Their experimental results indicated that the apparent activation energy of this reaction could be 324 or 424 kJ/mol in the inert atmosphere. However, the mathematical formula of the reaction kinetic mechanism and the value of pre-exponential factor haven't been reported.

The kinetic triplet contains the pre-exponential factor, activation energy and the reaction model function. To provide additional insight into the thermal decomposition of hematite ore, the kinetic triplet is calculated in this work.

2. Raw Material and Experimental Methods

Commercial hematite ore was supplied by Tata Steel IJmuiden. The average size of the hematite ore particles is 110.5 μm. The chemical and phase composition of the particles, which were determined by X-Ray fluorescence and diffraction facilities (XRF and XRD), are shown in **Table 1** and **Fig. 1**, respectively. The chemical composition in Table 1 is in the form of oxides with lacking of carbon content in the ore, which is equivalent to the composition of the calcined sample. It shows that minerals other than iron oxide are relatively abundant. High weight ratio of $(SiO_2+Al_2O_3)$/

Table 1. Normalized chemical composition of the calcined hematite ore particles in the form of oxide by XRF detection.

Name	Fe_2O_3	SiO_2	Al_2O_3	CaO	MgO	MnO	TiO_2	Rest.
(wt%)	72.354	14.03	4.985	2.974	2.524	1.429	0.721	0.985
Error	0.1	0.1	0.07	0.05	0.05	0.04	0.03	0.058

* Corresponding author: E-mail: aha_c@126.com
DOI: https://doi.org/10.2355/isijinternational.ISIJINT-2019-129

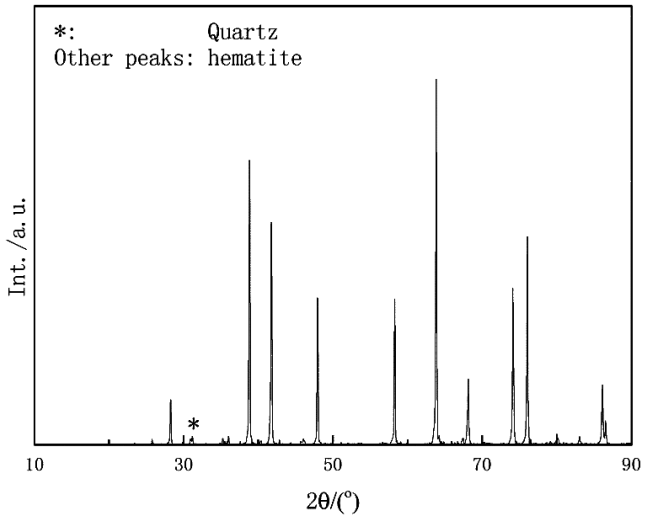

Fig. 1. XRD pattern of the particle with mean size of 110.5 μm.

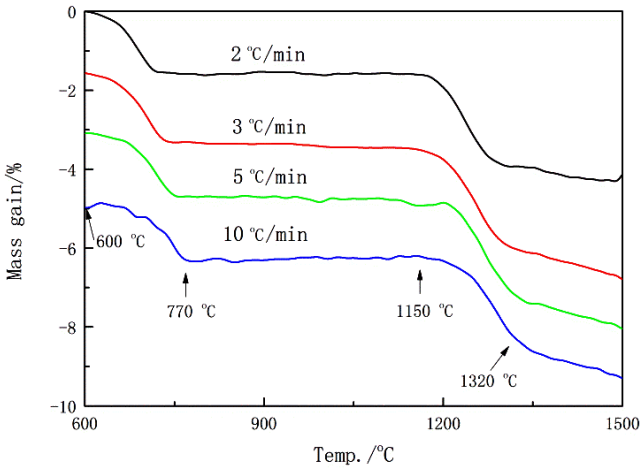

Fig. 2. Weight loss of hematite ore particles in temperature program reaction with different temperature rising rates in pure nitrogen. (Online version in color.)

(CaO+MgO) indicates it is an acid iron ore. Figure 1 shows that the principal phase is hematite. SiO_2 in the form of quartz is also shown in the XRD pattern.

Thermogravimetric analyzer (Netzsch Thermal Analysis STA 409) was used to study the thermal decomposition kinetics of the dried hematite ore particles. Around 20 mg of sample was put in a cylindrical crucible, linearly heated to a certain temperature. The heating rate was controlled as 2, 3, 5 and 10°C/min, respectively. Pure nitrogen was introduced into the reactor chamber in a flow rate of 40 ml/min. The reacted sample was cooled down naturally in the reactor after reaction. Part of the sample was collected for XRD, optical microscopy and scanning electron microscopy (SEM) observation. In SEM analysis, method of backscattered electrons (BSE) was combined with energy dispersive spectrometry (EDS) to provide details of the elements distribution of the particles.

3. Results and Discussion

3.1. Reaction Process

Figure 2 shows the thermogravimetric curves as illustration. The weight loss of hematite ore can be divided into two parts, recorded as low and high-temperature regions. In the experiment with the heating rate of 10°C/min, sample weight lost 1.61±0.17 wt% from 600 to 770°C. It is suggested that the low-temperature region is corresponding to the decomposition of carbonates (also known as calcination). The decomposition temperature of magnesite is from 267 to 540°C, calcite is from 720 to 780°C,[18] dolomite is above 770°C and contains two differential thermal analysis peaks.[19] Therefore, the carbonate is supposed to be calcite, and the decomposition reaction:

$$CaCO_3 = CaO + CO_2 \quad \text{..... (1)}$$

The amount of $CaCO_3$ is estimated to be 3.66±0.39 wt%. After the removal of CO_2 from the raw materials, the content of hematite in ore is 72.354 wt% as shown in Table 1. The weight loss of the sample in the reduction from hematite to magnetite, wustite and metallic iron are 2.41, 7.23 and 21.7 wt% of the calcined sample weight, w_0.

Figure 2 also indicates the thermal decomposition of hematite starts from 1 150°C, in the high temperature region. Around 3 wt% weight is lost in this region. The region can be divided into two stages, one is from around 1 150°C to 1 320°C, and the other is above 1 320°C. The turning point at 1 320°C implies a transformation of reaction kinetic mechanism. The weight losses at the turning points of all experiments are slightly lower than 2.41 wt% of the calcined sample. Since the reduction from hematite to magnetite losses 3.33 wt% of total weight as mentioned before, the experimental result indicates that the product can be principally magnetite rather than wustite or metallic iron.

Thermodynamics software, FactSage 7.0, was employed to predict the product composition in equilibrium. In the TGA experiments, gaseous products would be taken away from the reactor chamber by flowing nitrogen. Thus, a simulation of an open system was carried out for the thermodynamic prediction. In this open system, 1 L nitrogen was introduced into 100 g calcined Hematite ore with the same composition as Table 1. After the reaction achieved the equilibrium state, all gases, including the gaseous products, were removed from the reaction system, and then 1 L fresh nitrogen was introduced again for further reaction. The refreshing step was set to be 200 times in the simulation, and the total input amount of nitrogen was 200 L. **Figure 3** exemplifies the reaction products in equilibrium state at 1 450°C. Occurrence of iron oxides in the solid state is Spinel principally, and the total iron content in slag is around 11 to 17 wt%. Here, the spinel is the solid solution in which magnetite is the principal component. As predicted earlier, no metallic iron is produced in the thermal decomposition reaction. The prediction of the thermal decomposition of the ore in the open system (**Fig. 4**) shows that the amount of the released oxygen from the ore reaches 1.69, 5.08, and 15.50 L oxygen gas when the ore was decomposed to Fe_3O_4, FeO, and Fe, respectively. The oxygen emission in the decomposition is less than 5.08 L (The oxygen is 7.25 wt% of the calcined sample), which implies that the final products of thermal decomposition are principally magnetite, with mixing of some FeO. Figures 3 and 4 both show the equilibrated composition varies not only with nitrogen volume but also with the reaction temperature. Therefore, the weight loss at the reaction termination point

needs to be assumed based on the comprehensive survey of experimental results and thermodynamic theory.

3.2. Characterizations of the Reacted Sample during the Reaction

In Fig. 2, there are two temperature regions with three steps of weight loss. Therefore, the specimens at room temperature, 1 100°C, 1 310°C and 1 500°C were observed by BSE/EDS. The three temperatures are located within different ranges of the three steps. The surface morphology of the particles is shown in **Fig. 5**, and the cross section is shown in **Fig. 6**. The color of hematite phase in the figures is light and other minerals are dark. Figure 5(a) shows that most hematite particles contain no or very few other minerals inside. EDS data shows that the main cation in non-hematite particles is silicon cations. In addition, SiO_2 (quartz) was detected as a single phase. All other non-hematite oxides seem to be complex oxides. Besides, EDS data shows few or none iron in the complex oxides. After heated to 1 100°C, the thermal decomposition of hematite did not start, but carbonates had already been burnt into oxides. Due to the calcination, the surface of some non-hematite particles has been crisscrossed by cracks (Fig. 5).

The samples reached 1 310°C and 1 500°C were scraped from the agglomerations in the crucible. Figures 5(c) and 6(b) show that the non-hematite oxides have melted, forming considerable amount of slag as connectors of two particles. Usually, the reactants prefer to diffuse through a thin gas boundary layer rather than a sticky slag phase. Comparing to the release of oxygen happens between gas-particle surface, it is assumed that the reaction rate on the

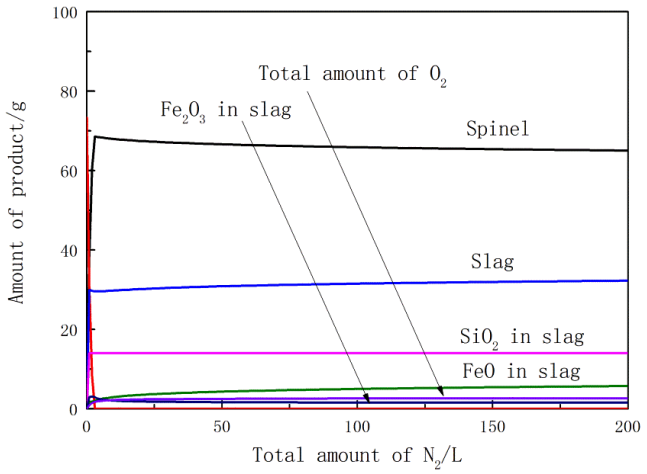

Fig. 3. Equilibrium state of 100 g Hematite ore particles reacted with nitrogen in open system at 1 450°C. (Online version in color.)

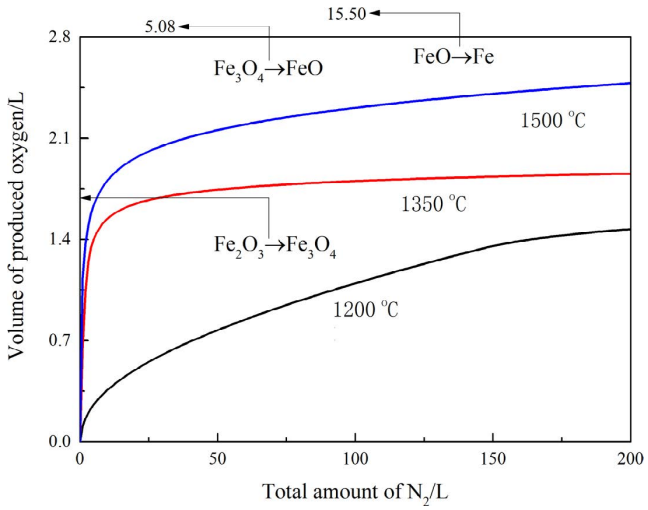

Fig. 4. Total released oxygen in equilibrium state of 100 g Hematite ore particles reacted with nitrogen in open system, where the values above the frame of the diagram show the amount of released oxygen gas at the end of the corresponding reactions. (Online version in color.)

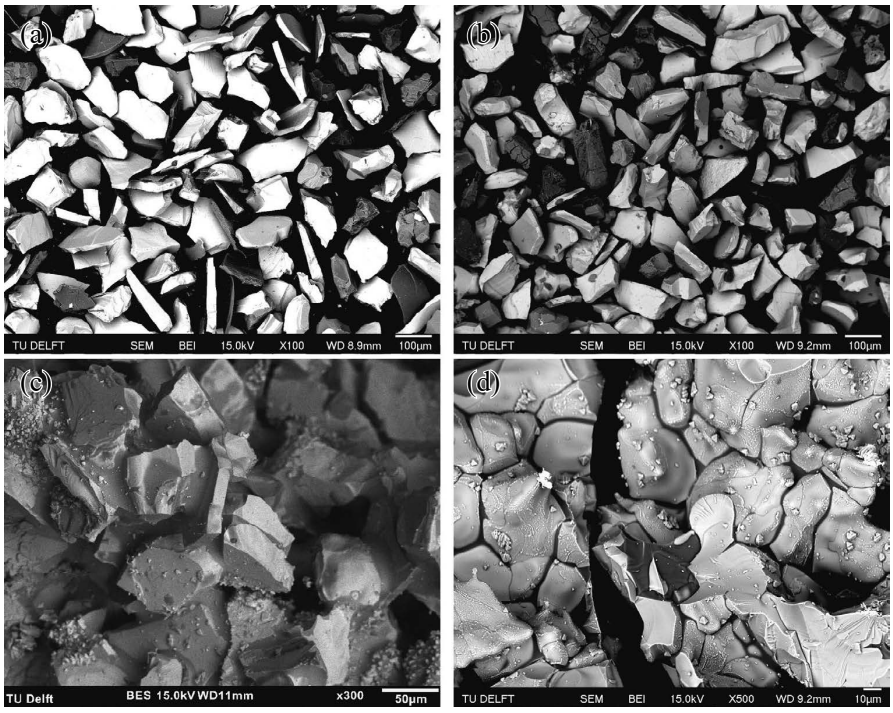

Fig. 5. Surface morphology of Hematite ore particles at (a) room temperature; (b) 1 100°C; (c) 1 310°C; (d) 1 500°C.

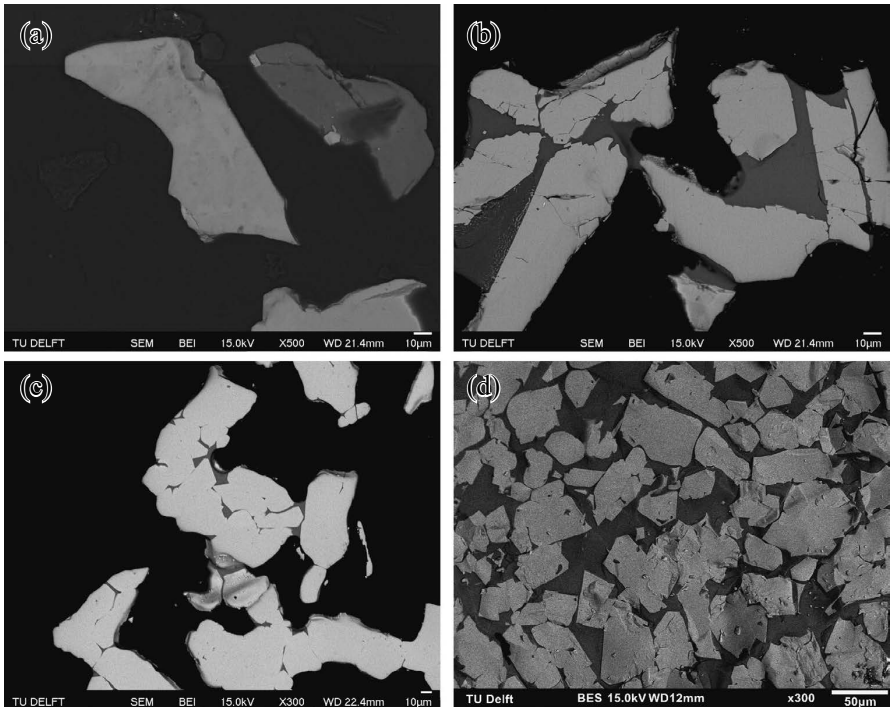

Fig. 6. Cross section of Hematite ore particles reached (a) 1 100°C; (b) 1 310°C; (c) 1 500°C (stripped particles); (d) 1 500°C (bottom in the crucible).

slag-particle interface could be ignorable. Therefore, the real reaction interface at the high temperatures was reduced by slag formation.

Figures 6(c)–6(d) show the hematite particles breaking up into small pieces, which could be a result of the deformation stress in the reduction process. Due to the increased gas-ore interface, the reduction rate should increase, however, Fig. 2 shows an opposite result. The figures also indicate that, at high temperature, molten slag flowed down to the bottom of the alumina crucible, leaving less slag on the top. Such top part (Fig. 6(c)) is relatively easier to be stripped off for observation. The ore particles at the bottom (Fig. 6(d)) were submerged in bulk slag, therefore the reaction surface of the bottom part was very limited. The figures show that the plasticity of particles was stronger at the higher temperatures. Therefore, the deformed particles on the top of the crucible were merged by the small amount of slag as connectors of the matching surfaces. The reaction surface of the top part was also limited. As a result, the reduction rate decreased at 1 500°C.

Slag composition was detected by EDS. It shows that silicon cations range from 26 to 30 mol% at 1 500°C. 3 to 5 mol% of iron cations were detected out in the slag at 1 310°C, which implied the interaction between slag and ore particles was limited. However, 5 to 10 mol% of iron cations contents in slag at 1 500°C. The increasing iron concentration in slag implies that the interaction between slag and ore particles is more important at higher temperature.

The XRD analysis results of the reacted samples are given in **Fig. 7**. Only hematite and quartz were detected at 1 100°C. At 1 310°C, around 42.4 wt% of hematite had been reduced to be magnetite based on the semi quantitative analysis.[20] No hematite was detected at 1 500°C. The diffuse X-ray peak around 20° at 1 310°C and 1 500°C is contributed by the slag phase. The XRD results suggest that

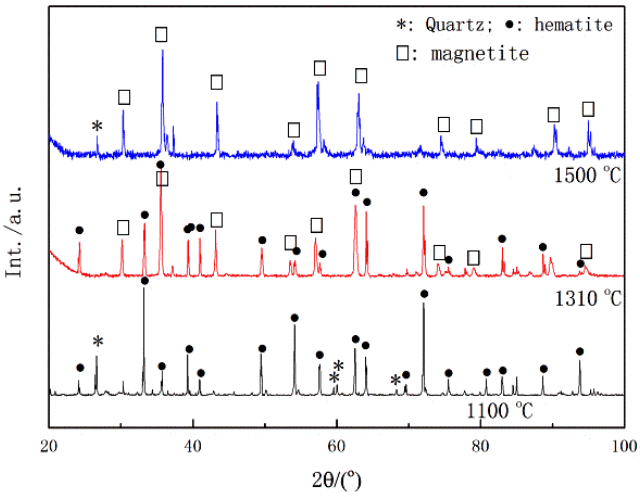

Fig. 7. XRD pattern of Hematite ore particles before and after reaction with heating rate of 10°C/min to different temperatures. (Online version in color.)

the thermal decomposition from hematite to magnetite has been finished before 1 500°C. At the meantime, the melting already started.

3.3. Kinetic Parameters of Thermal Decomposition

Iso-conversional methods are employed to obtain the activation energies of the two kinetic stages of thermal decomposition. The two stages are divided by the turning point of 1 320°C. Three iso-conversional methods, Kissinger method, Ozawa-Flynn-Wall method and Boswell method, were compared to verify the results. These methods are well known as a model-free kinetic approach. All the methods are based on the numerical solution of the temperature integration. The general equation of all the three methods

is as follows:[21]

$$\ln\frac{\beta g(\alpha)}{T_f^s}=\frac{B\Delta E}{RT_f}+\mathrm{C} \quad \text{..... (2)}$$

where, $g(\alpha)$ is the integral form of the mathematical function that represents the reaction mechanism, α is the reaction fraction, β is the temperature-increasing rate, R is gas constant, ΔE is the apparent activation energy, T_f is the temperature at a fixed state of transformation and B and s are constants. In the case of Kissinger's method $s=2$, and $B=1$, for Boswell[22] $s=1$, and $B=1$, and for Ozawa-Flynn-Wall method[23] $s=0$, and $B=1.0518$. The requirement of the method application is $15\le\frac{\Delta E}{RT_f}\le 60$. Ozawa-Flynn-Wall method is employed to compute the pre-exponential factor, A, in Arrhenius law:

$$k=A\exp\left(-\frac{\Delta E}{RT}\right) \quad \text{..... (3)}$$

Where, k is the reaction rate constant, and it is known that in Eq. (2) $\mathrm{C}=\ln[AR/(g(\alpha)\ \Delta E)]-5.3305$.[23] It could be noticed that the pre-exponential factor cannot be calculated out directly from the aforementioned methods because of the unknown formula of $g(\alpha)$. However, using compensation effect, the value of A can be estimated following the evaluation of activation energy. The calculation result is shown in **Fig. 8**. Here, the $\Delta w/w_0$ is set to be 0% at the start point of thermal decomposition reaction. $\Delta w/w_0$ is defined as the weight loss of the sample divided by the total weight of calcined sample. The value of adj. R^2 is used to judge the linearity of the data. The degree of linearity of the 2nd stage is weaker according to the lower value of adj. R^2 comparing to the 1st stage. An average value of the reaction activation energy for the 1st stage is 629±75, 636±75 and 648±74 kJ/mol according to Kissinger method, Ozawa-Flynn-Wall method and Boswell method, respectively. The ΔE for the 2nd stage is 313±42, 325±38 and 327±41 kJ/mol according to different methods in sequence. The experimental data with heating rate of 2°C/min is excluded from the kinetic analysis for the 2nd stage for that it cannot fulfill the requirement of calculation. It is noted that the activation energies for the iron oxides thermal decomposition at high temperature is higher than that of low temperature reduction (below 1 150°C).[5] Salmani *et al.*[17] suggest the thermal decomposition of hematite could be controlled by chemical reaction, which coincides with Qu.'s view.[14,16] Especially, comparably, the activation energy of cations inside the matrix can contribute to such high activation energy. Based on the values on the values of activation energies and the literatures, it implies that the rate controlling steps in both first stage and second stage can be the inner diffusion step of iron in solid phase and the diffusion of iron in slag phase, respectively. Whilst, experimental works with advanced characterization of the microstructure development of the samples need to be carried out to further clarify the reaction kinetic mechanism.

The values obtained via Ozawa-Flynn-Wall method are selected for the next analysis. It is know that the compensation effect of A and ΔE is:[24,25]

$$\ln A=\frac{\Delta E}{RT}+\ln\left[\frac{d\alpha/dt}{f(\alpha)}\right]=a+b\Delta E \quad \text{..... (4)}$$

where, $f(\alpha)$ is the differential form of the mathematical function that represents the reaction mechanism, a and b are the two compensation parameters. It indicates a linear relationship of a pair of apparent Arrhenius parameters. Based on Eq. (4), A can be calculated out if we know the value of the other three in the equation. No matter what model is used to describe the actual reaction kinetics, the values of the compensation parameters should be the same. Therefore, all the possible models, even if they cannot describe the real reaction kinetics, could be employed to fit the experimental data to get several pairs of A and ΔE, then the values of a and b could be obtained from a linear relationship of them. According to this linear relationship, the value of A could be evaluated from the known ΔE.

The differential forms, $f(\alpha)$, and integral forms, $g(\alpha)$, of some potential kinetic models are listed in **Table 2**. All of them were fitted to the experimental data using Achar-Brindley-Sharp's differential method.[26] The equation of this method is described as follows:

$$\ln\left(\frac{d\alpha}{dt}\right)-\ln f(\alpha)=\ln A-\frac{\Delta E}{RT} \quad \text{..... (5)}$$

It is noticed that the derivative of the reaction fraction, α, is necessary for the calculation. Also, α has to be defined before fitting. Theoretically, it is assumed that the weight loss of ore particles is 2.41 wt% of the calcined sample at

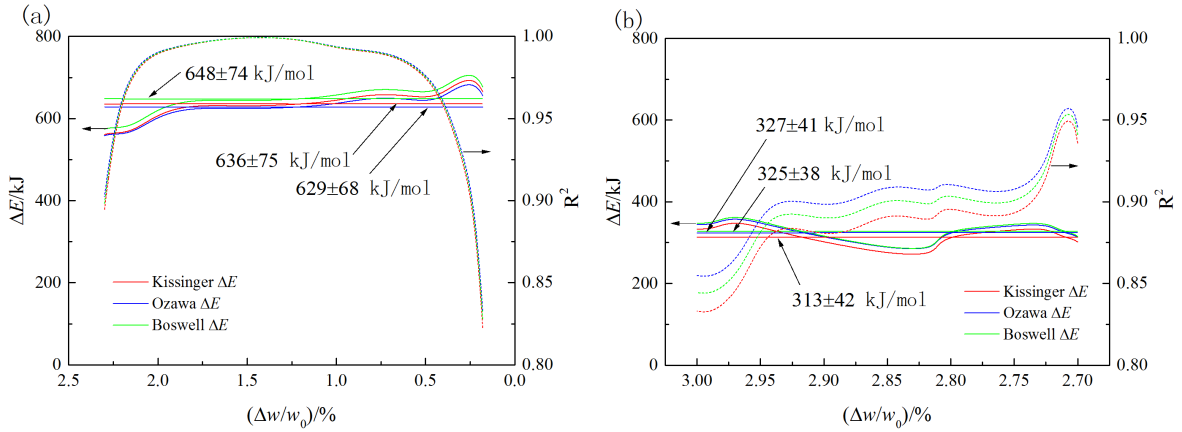

Fig. 8. Activation energy of thermal decomposition reaction: (a) 1st stage; (b) 2nd stage, which are before and after 1 320°C. (Online version in color.)

Table 2. The kinetic models of heterogeneous reactions.

Reaction model	Code	f(α)	g(α)
Power law	P1	$4\alpha^{3/4}$	$\alpha^{1/4}$
Power law	P2	$3\alpha^{2/3}$	$\alpha^{1/3}$
Power law	P3	$2\alpha^{1/2}$	$\alpha^{1/2}$
Power law	P4	$2/3\alpha^{-1/2}$	$\alpha^{3/2}$
One-dimensional diffusion	D1	$1/2\alpha^{-1}$	α^{2}
Mampel (first order)	F1	$1-\alpha$	$-\ln(1-\alpha)$
Avrami-Erofeev	A4	$4(1-\alpha)[-\ln(1-\alpha)]^{3/4}$	$[-\ln(1-\alpha)]^{1/4}$
Avrami-Erofeev	A3	$3(1-\alpha)[-\ln(1-\alpha)]^{2/3}$	$[-\ln(1-\alpha)]^{1/3}$
Avrami-Erofeev	A2	$2(1-\alpha)[-\ln(1-\alpha)]^{1/2}$	$[-\ln(1-\alpha)]^{1/2}$
Three-dimensional diffusion	D3	$3/2(1-\alpha)^{2/3}$ $[1-(1-\alpha)^{1/3}]^{-1}$	$[1-(1-\alpha)^{1/3}]^2$
Contracting sphere	R3	$3*(1-\alpha)^{2/3}$	$1-(1-\alpha)^{1/3}$
Contracting cylinder	R2	$2*(1-\alpha)^{1/2}$	$1-(1-\alpha)^{1/2}$
Two-dimensional diffusion	D2	$[-\ln(1-\alpha)]^{-1}$	$(1-\alpha)\ln(1-\alpha)+\alpha$
Second order	F2	$(1-\alpha)^2$	$(1-\alpha)^2$

the end of the 1st reaction stage, when the hematite phase has been converted to magnetite; and 7.23 wt% at the 2nd reaction stage, when the sample has been converted to Fe^{3+}-free molten slag. Furthermore, α is defined to be the real weight loss of the sample in the thermal decomposition reaction divided by this theoretical weight loss. Before derivation, a smooth of the curve to reduce the noise could also result in data distortion. This negative effect has been reduced to an acceptable range. The experimental data was transferred to be the form of the left side of Eq. (5), then the corresponding values of A and ΔE for each model were evaluated by linear fitting. The fitting results of the reaction with temperature rising rate of 2°C/min are shown in **Fig. 9** as an illustration. **Table 3** shows that the fitting results of adj. R^2 varies from 0.26 to 0.99. The model with higher value of adj. R^2 implies a potential reaction kinetics, but the fitting results show either several models have similar values of adj. R^2, or the model with the highest value of adj. R^2 is inconsistent in different experiments. Although no model can be suggested to be the best one, in synthesis, the reaction models with codes of F1, F2 and D3 could be the candidates of the potential kinetic mechanism.

Based on the fitting results, the relationship of A and ΔE was built up as shown in **Fig. 10**. The value of A was estimated from the value of ΔE that was obtained by Ozawa-Flynn-Wall method. Usually, the correct A and ΔE could be figured out by the intersect point of the compensation lines with different temperature rising rates.[27,28] However, the difference of the slopes of the four lines in Fig. 10 is so small that it could be ignored considering the computational error. Therefore, the value of A is better to be estimated from the mean value of the slopes rather than from the intersect point of the lines. Take the compensation line with 2°C/min as an illustration, the values of a and b are -11.86 and $8.11\cdot10^{-5}$ mol/J, respectively. And the value of $\ln(A/s^{-1})$ can be calculated as 43.5 ± 6.1. Overall, the average value of $\ln(A/s^{-1})$

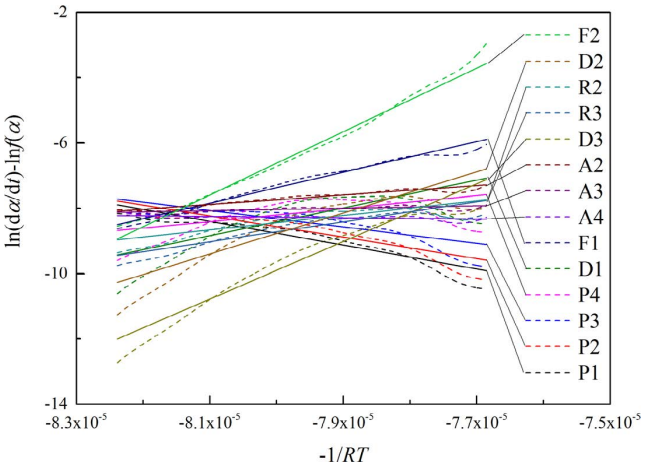

Fig. 9. Fitting results of kinetic models to the thermal decomposition of hematite ore in nitrogen atmosphere, where the dash lines are the experimental data, and the solid lines are the fitting results of Achar-Brindley-Sharp's equation with temperature rising rate 2°C/min. (Online version in color.)

Table 3. Value of adj. R^2 for the models in Fig. 9.

Model	Adj. R-Square			
	2°C/min	3°C/min	5°C/min	10°C/min
P1	0.8674	0.7546	0.9167	0.7204
P2	0.8218	0.6381	0.8738	0.6352
P3	0.6822	0.2642	0.7010	0.4003
P4	0.3141	0.7753	0.6678	0.5134
D1	0.5884	0.8615	0.8007	0.7054
F1	0.9779	0.9877	0.9716	0.9748
A4	0.2594	0.8091	0.2838	0.4258
A3	0.5101	0.8912	0.5815	0.7037
A2	0.9232	0.9519	0.8432	0.8903
D3	0.9430	0.9939	0.9815	0.9638
R3	0.8588	0.9890	0.9606	0.9029
R2	0.6847	0.9683	0.9249	0.8035
D2	0.8115	0.9550	0.9258	0.8710
F2	0.9891	0.9440	0.9453	0.9743

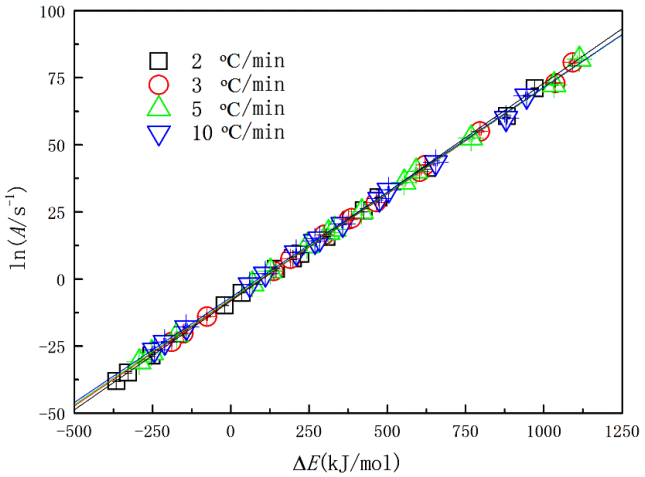

Fig. 10. Compensation effect of A and ΔE in the 1st stage of thermal decomposition reaction. (Online version in color.)

is 42.9±6.6 for the whole experiments.

Similarly, for the 2nd stage of thermal decomposition reaction, one could find the compensation effect of A and ΔE, which is shown in **Fig. 11**. It could be noticed that the error bars are greatly increased comparing with the data in Fig. 10. It is because of its relatively low reaction rate and excessive ambient noise. The values of a and b in Eq. (4) are -10.49 and $7.51\cdot10^{-5}$ mol/J, respectively. Furthermore, the value of $\ln(A/s^{-1})$ is estimated to be 14.1±3.08.

3.4. Discussion of Reaction Mechanism

The study objective is to provide values of kinetic triplet to the thermal decomposition of particles in the cyclone converter in HIsarna reactor. The 1st stage of the thermal decomposition in TGA is similar to the pre-reduction of particle suspension in the cyclone with high load of ore, where the melted slag phase could join the ore particles as clusters. The 2nd stage can be regarded as the reaction of gas and the slag on the wall of cyclone.

Since the values of ΔE and A are known, the kinetic model of the reaction could be estimated by comparison with the experimental data. The values of ΔE and A were substituted into the equations of kinetic models in Table 2, and the corresponding curves are plotted in **Fig. 12**. It shows that the models in Table 2 could not be used to describe the reaction mechanism. Especially, it can be noted an obvious deviation between the experimental data and the models F1, F2 and D3. In this situation, Sestak-Berggren (SB) model[29,30] is suggested to be employed:

$$f(\alpha)=\alpha^m(1-\alpha)^n \quad \text{..... (6)}$$

where, m and n are empirical parameters. Fitting process was carried out with flexible value of $\ln A$, and the result is shown in Fig. 12. And the expression of reaction rate could be as follows:

$$\frac{d\alpha}{dt}=\exp\left(42.9-10^3\cdot\frac{636}{RT}\right)\cdot(1-\alpha)^{1.38} \quad \text{..... (7)}$$

This formula is similar to the Mampel mechanism (code F1), but the integral form of it has no analytical solution. Moreover, based on Eq. (7), one can predict the thermal decomposition reaction of the ore particles in HTDF or HIsarna reactor.

Figure 13 shows the prediction results of isothermal reactions based on Eq. (7), the kinetic model of the 1st stage of thermal decomposition. Comparing to the known experimental results in nitrogen gas from Qu *et al.*,[31] it can be noticed that the predicted data at 1 527°C is similar to the reported data. Nevertheless, the predicted data at 1 377°C is much lower than her data at the same reaction time. Accordingly, it is easy to know that the value of activation energy in this experiment is higher than the reference data. The reason could be the different chemical compositions and structures of the raw materials. More characterization for different ore particles needs to be carried out in the future to comprehensive understanding.

The relatively excessive noise in the 2nd stage of thermal decomposition effects the result a lot, which results in that one cannot point out the proper reaction kinetic model properly. As shown in **Fig. 14**, it could only be recommended that F2 might be the potential kinetic equation of the reaction at this stage.

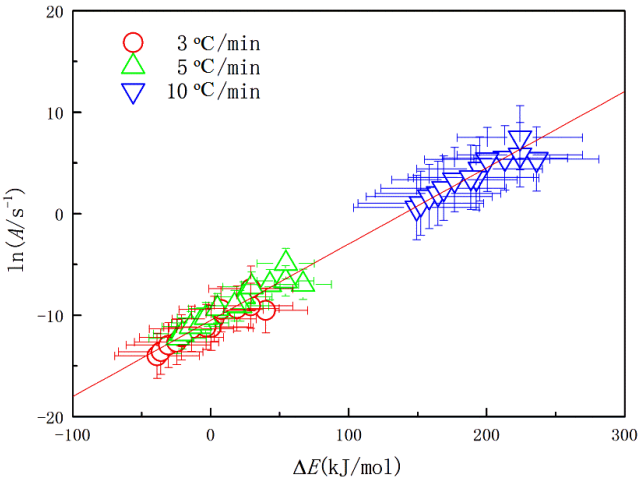

Fig. 11. Compensation effect of A and ΔE in the 2nd stage of thermal decomposition reaction. (Online version in color.)

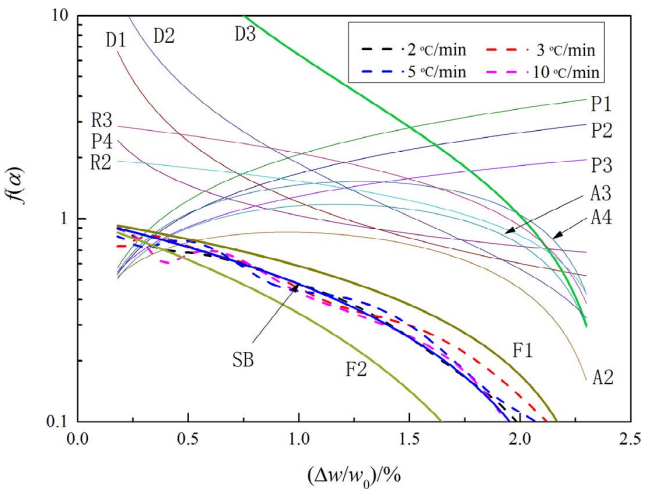

Fig. 12. The $f(\alpha)$ values estimated for the 1st stage of Hematite ore thermal decomposition with different heating rate. The dash lines are experimental results, and the solid lines represent the theoretical models. (Online version in color.)

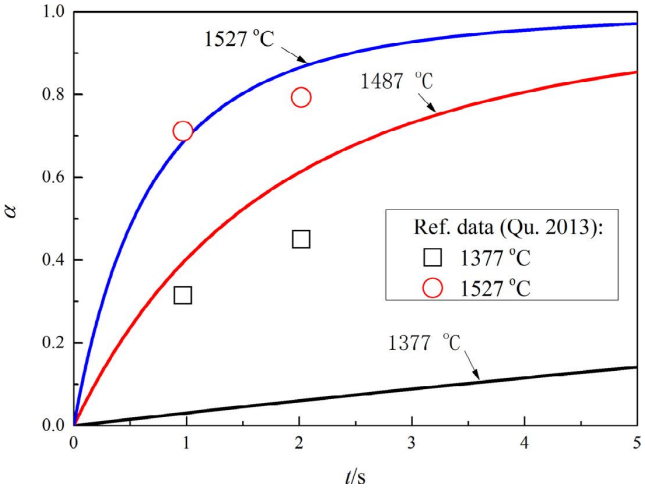

Fig. 13. Prediction of isothermal reaction kinetic curves from model (7) and the experimental results from reference.[7] (Online version in color.)

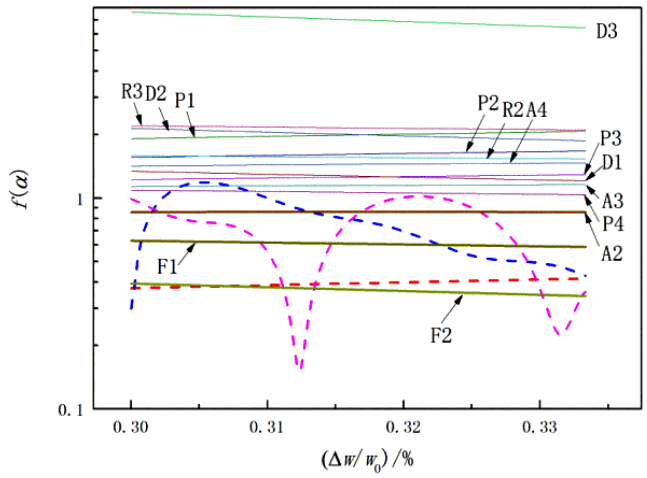

Fig. 14. The $f(\alpha)$ values estimated for the 2nd stage of Hematite ore thermal decomposition with different heating rate. The dash lines are experimental results, and the solid lines represent the theoretical models. (Online version in color.)

4. Conclusions

(1) The thermal decomposition of hematite ore starts from 1 150°C, and it contains two kinetic stages. The weight loss of the sample with average particle size contribution of 110.5 μm is within 2.41 wt% in the 1st stage. And the XRD data shows that the decomposed sample contains magnetite principally.

(2) Slag forms in the reaction, which results in slowing down of the reaction rate in the 2nd stage. Based on the thermodynamic prediction, the slag composition contains Fe^{2+} and Fe^{3+}, and the iron cations concentration nearly doubled from 1 310°C to 1 500°C. However, Si^{4+} is the principal component in the slag.

(3) The reaction mechanism of the 1st thermal decomposition stage is proposed to be the inner diffusion step of iron in solid phase. Moreover, the reaction mechanism of the 2nd stage could be the diffusion of iron in slag phase.

(4) The kinetics of the thermal decomposition reaction in 1st stage was analyzed based on the isoconversional method. The values of $\ln(A/s^{-1})$, ΔE and $f(\alpha)$ are proposed to be 42.9, 636 kJ/mol, and $(1-\alpha)^{1.38}$, respectively.

(5) The values of $\ln(A/s^{-1})$ and ΔE of the thermal decomposition reaction in 2nd stage are proposed to be 14.1 and 325 kJ/mol, respectively.

Acknowledgments

This research was carried out at Delft University of Technology and was financially supported by the Materials innovation institute M2i (www.m2i.nl) under the project T41.5.13489. The authors would like to express their thanks to Dr. Sripriya Rajendran and Mr. Jelle Agema from Tata Steel Europe (IJmuiden) for fruitful discussions for this study. Ruud Hendrikx at the Department of Materials Science and Engineering of the Delft University of Technology is acknowledged for the X-ray analysis.

REFERENCES

1) E. R. Monazam, R. W. Breault and R. Siriwardane: *Energy Fuel.*, **28** (2014), 5406.
2) J. Janowski and A. Sadowski: *Ironmaking Steelmaking*, **23** (1996), 479.
3) Y. Kashiwaya, Y. Yamaguchi, H. Kinoshita and K. Ishii: *ISIJ Int.*, **47** (2007), 226.
4) P. Hayes and P. Grieveson: *Metall. Trans. B*, **12** (1981), 579.
5) A. Pineau, N. Kanari and I. Gaballah: *Thermochim. Acta*, **447** (2006), 89.
6) K. Meijer, C. Zeilstra, C. Teerhuis, M. Ouwehand and J. van der Stel: *Trans. Ind. Inst. Met.*, **66** (2013), 475.
7) Y. Qu: Ph.D. thesis, Delft University of Technology, (2013), https://repository.tudelft.nl/islandora/object/uuid%3A7189ac3e-a887-48a6-90cb-07a1f17918aa, (accessed 2013-09-03).
8) S. Story, B. Sarma, R. Fruehan, A. Cramb and G. Belton: *Metall. Mater. Trans. B*, **29** (1998), 929.
9) B. Sarma, A. Cramb and R. Fruehan: *Metall. Mater. Trans. B*, **27** (1996), 717.
10) D. Q. Fan, H. Y. Sohn, Y. Mohassab and M. Elzohiery: *Metall. Mater. Trans. B*, **47** (2016), 3489.
11) M. Choi and H. Sohn: *Ironmaking Steelmaking*, **37** (2010), 81.
12) F. Tsukihashi, K. Kato, K.-i. Otsuka and T. Soma: *Tetsu-to-Hagané*, **68** (1982), 750 (in Japanese).
13) N. Takeuchi, Y. Nomura, K.-i. Ohno, T. Maeda, K. Nishioka and M. Shimizu: *ISIJ Int.*, **47** (2007), 386.
14) Y. Qu, Y. Yang, Z. Zou, C. Zeilstra, K. Meijer and R. Boom: *ISIJ Int.*, **55** (2015), 952.
15) Y. Qu, Y. Yang, Z. Zou, C. Zeilstra, K. Meijer and R. Boom: *ISIJ Int.*, **55** (2015), 149.
16) Y. Qu, Y. Yang, Z. Zou, C. Zeilstra, K. Meijer and R. Boom: *Ironmaking Steelmaking*, **42** (2015), 763.
17) M. Salmani, E. K. Alamdari and S. Firoozi: *J. Therm. Anal. Calorim.*, **128** (2017), 1385.
18) H. Britton, S. Gregg and G. Winsor: *Trans. Faraday Soc.*, **48** (1952), 63.
19) R. McIntosh, J. Sharp and F. Wilburn: *Thermochim. Acta*, **165** (1990), 281.
20) F. Chung: *J. Appl. Crystallogr.*, **7** (1974), 519.
21) M. Starink: *Thermochim. Acta*, **288** (1996), 97.
22) P. Boswell: *J. Therm. Anal. Calorim.*, **18** (1980), 353.
23) T. Ozawa: *Thermochim. Acta*, **203** (1992), 159.
24) N. Sbirrazzuoli: *Thermochim. Acta*, **564** (2013), 59.
25) S. Vyazovkin: Isoconversional Kinetics of Thermally Stimulated Processes, Springer, New York, (2015), 41.
26) B. N. Achar, G. Brindley and J. Sharp: Proc. Int. Clay Conf., Israel Program for Scientific Translations, Jerusalem, (1966), 67.
27) S. Vyazovkin and A. Lesnikovich: *Thermochim. Acta*, **128** (1988), 297.
28) A. Lesnikovich and S. Levchik: *J. Therm. Anal. Calorim.*, **27** (1983), 89.
29) S. Vyazovkin, A. K. Burnham, J. M. Criado, L. A. Pérez-Maqueda, C. Popescu and N. Sbirrazzuoli: *Thermochim. Acta*, **520** (2011), 1.
30) J. Šesták and G. Berggren: *Thermochim. Acta*, **3** (1971), 1.
31) Y. Qu, Y. Yang, Z. Zou, C. Zeilstra, K. Meijer and R. Boom: *ISIJ Int.*, **54** (2014), 2196.